Marine Pollution Bulletin 90 (2015) 259–272

Contents lists available at ScienceDirect

Marine Pollution Bulletin

journal homepage: www.elsevier.com/locate/marpolbul

Oil spill hazard from dispersal of oil along shipping lanes in the Southern Adriatic and Northern Ionian Seas

S. Liubartseva [a,*], M. De Dominicis [b], P. Oddo [b], G. Coppini [c], N. Pinardi [d], N. Greggio [e]

[a] Centro EuroMediterraneo sui Cambiamenti Climatici, Bologna, Italy
[b] Istituto Nazionale di Geofisica e Vulcanologia, Bologna, Italy
[c] Centro EuroMediterraneo sui Cambiamenti Climatici, Lecce, Italy
[d] Department of Physics and Astronomy, University of Bologna, Italy
[e] Italian Coast Guard Headquarters, Ministry of Infrastructures and Transports, Rome, Italy

ARTICLE INFO

Article history:
Available online 14 November 2014

Keywords:
Oil spill modelling
Hazard mapping
Operational oil pollution
Southern Adriatic and Northern Ionian Seas

ABSTRACT

An assessment of hazard stemming from operational oil ship discharges in the Southern Adriatic and Northern Ionian (SANI) Seas is presented. The methodology integrates ship traffic data, the fate and transport oil spill model MEDSLIK-II, coupled with the Mediterranean Forecasting System (MFS) ocean currents, sea surface temperature analyses and ECMWF surface winds. Monthly and climatological hazard maps were calculated for February 2009 through April 2013. Monthly hazard distributions of oil show that the zones of highest sea surface hazard are located in the southwestern Adriatic Sea and eastern Ionian Sea. Distinctive "hot spots" appear in front of the Taranto Port and the sea area between Corfu Island and the Greek coastlines. Beached oil hazard maps indicate the highest values in the Taranto Port area, on the eastern Greek coastline, as well as in the Bari Port area and near Brindisi Port area.

1. Introduction

Although accidental oil pollution caused by ships is decreasing, routine operational pollution has increased over the years (Pavlakis et al., 2001; Tarchi et al., 2006; Ferraro et al., 2007; Kirby and Law, 2010). Operational discharges from all ship types (cargo, tanker, ferry, passenger) include bilge water from machinery spaces, fuel oil sludge, and oily ballast water from fuel tanks.

In view of the current situation and the predicted increase (REMPEC, 2008) in ship traffic in the Mediterranean Sea and in particular the Southern Adriatic and Northern Ionian (SANI) region, it is mandatory to map the probability of exposure of local marine and coastal resources to oil pollution conditions. Hazard mapping appears to be the most appropriate way to approach the management of oil pollution in marine areas in order to sustain marine ecosystem health. State-of-the art hazard mapping should consider the intrinsic variability of the marine environment and should evaluate the sources of uncertainty in the system. Thus, effective risk management requires products that are time-dependent and that allow an almost continuous incorporation of the hydrodynamics systems' spatial and temporal variations.

In the context of natural hazards, the risk for a set of territorial elements is defined as a function of hazard, value, and vulnerability (UNESCO, 1972). Hazard refers to the likelihood that any particular area will be affected by a destructive event within a given period of time, value refers to the numbers and types of elements exposed to the destructive hazard, and vulnerability is a measure of the capability of the exposed elements to counteract the destructive effects of the event and thus refers to the proportion of value at stake for a given event. Operational pollution in shipping routes is a fluctuating hazard with a magnitude that changes dynamically as a result of a number of external parameters that vary in space and time (e.g., sea currents, waves, wind, sea surface temperatures).

Several studies were performed for different time periods and geographical areas to assess oil contamination hazards and environmental risks in terms of probability of impact in a certain area. Some previous studies integrated atmospheric and hydrodynamic datasets with the full oil spill transport and fate models (French et al., 1999; Abascal et al., 2010; Daniel et al., 2011; Singkran, 2013; Zelenke et al., 2012). Others used simplified oil spill models (Olita et al., 2012) or replaced oil by a system of passive tracers (Price et al., 2003, 2004; Galt and Payton, 1999; Barker and Galt, 2000; Samuels et al., 2013; Pizzigalli et al., 2007). Although in some studies oil spill models were not used (Ronza et al., 2006; Grifoll et al., 2010), they nonetheless suggested useful approaches to assess hazards and risks that arise from operational oil discharges

* Corresponding author.
E-mail address: svitlana.liubartseva@cmcc.it (S. Liubartseva).

http://dx.doi.org/10.1016/j.marpolbul.2014.10.039
0025-326X/

in ports. The relevant parameters of risk and hazard assessment, which are comparable with the parameters of the present work, are extracted from the literature cited above and summarized in Table 1.

In the present work, an original methodology of oil pollution hazard mapping was developed that differs from previous approaches in that it uses: (1) the UNESCO hazard definition, which has never before been used in oil spill modelling; (2) actual monthly ship traffic data provided by the Italian Coast Guard (ITCG); (3) ensemble runs of the oil spill model MEDSLIK-II (De Dominicis et al., 2013a,b), thereby avoiding any simplifications in the oil transport and weathering; and (4) operational analyses from the Mediterranean Forecasting System (MFS) service (Pinardi et al., 2003; Tonani et al., 2008; Oddo et al., 2009). The final objective is to use this methodology to evaluate surface and coastline oil contamination hazard in the SANI area (Fig. 1).

The manuscript is organized as follows: in Section 2 the data on ship traffic, the oil spill model, and the ocean forecasting system are presented; Section 3 is used to describe the methodology to estimate the oil quantity discharged from the ship traffic data, the setup of the oil spill model simulations, and the hazard calculation methodology; and Sections 4 and 5 contain descriptions of the results and conclusions, respectively.

2. Models and data

2.1. Shipping routes and traffic density data

In an effort to quantify and assess the hazards generated by operational oil discharges from ships, the first step was to collect data on shipping routes and traffic. The higher traffic density shipping routes in the SANI area were chosen based on monthly ship traffic density distributions data (January 2009–April 2013) provided by the Italian Coast Guard (ITCG) through the aggregation of real-time tracking of vessel positions via the Automatic Identification System (AIS). Ship traffic density is expressed as number of ships in the geographic coordinate per month. The ship traffic density is divided into 5 categories according to the number of passages per month: 5–6, 7–9, 10–14, 15–29, and more than 30. Despite the apparent similarity among the distributions of hypothetical oil spills (not shown), both monthly and yearly variability is present.

2.2. The oil spill model: MEDSLIK-II

The oil spill model code MEDSLIK-II (De Dominicis et al., 2013a,b) is a freely available community model (http://gnoo.bo.ingv.it/MEDSLIKII).

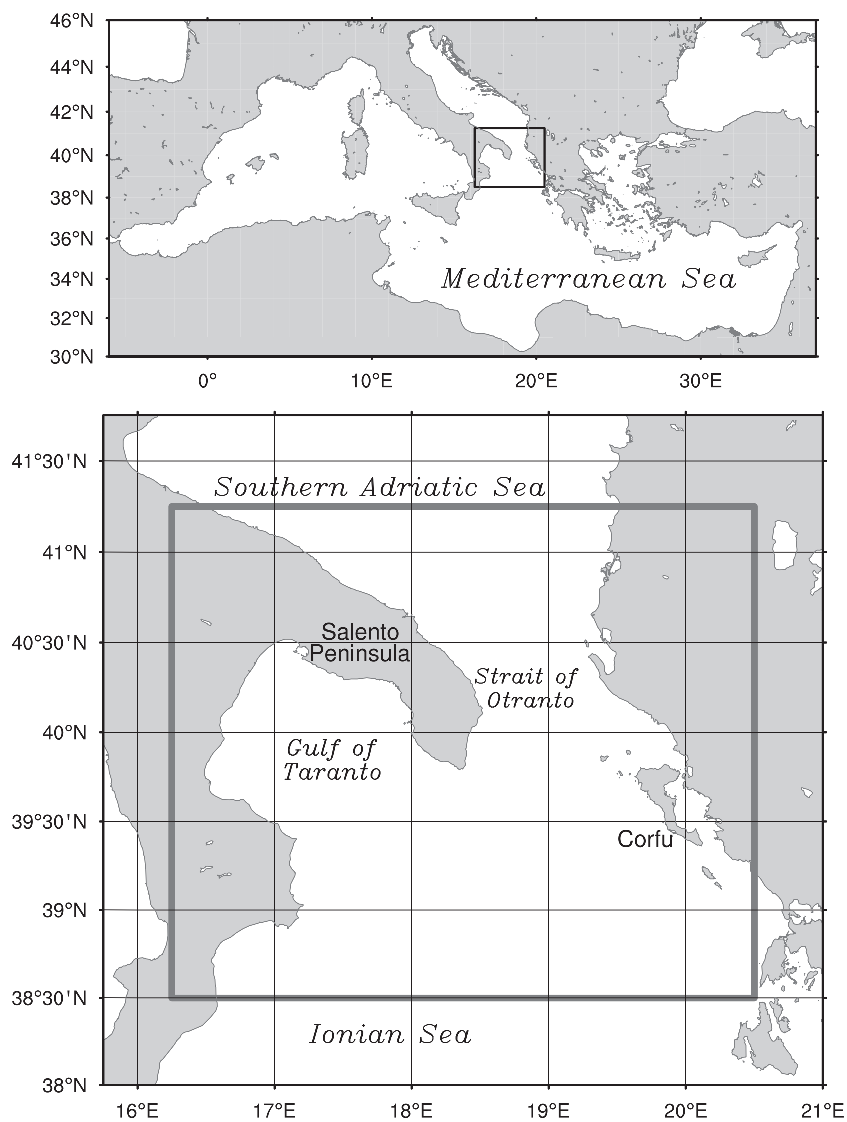

Fig. 1. SANI area.

Table 1
Relevant parameters on oil spill hazard and risk assessment.

Domain	Oil spill model reference	Number of individual runs	Notes
Tampa Bay, Florida	SIMAP (French et al., 1999)	50	Output on monthly and seasonal base from a seashore source
US continental shelf	OSRA (Price et al., 2003)	1000	3-, 10-, 30-day simulations from 100,000 hypothetical sources
San Francisco Bay	Passive tracers (Barker and Galt, 2000)	500	3-, 5-day simulations
Bay of Biscay and Cantabrian coastal area	PICHI (Abascal et al., 2010)	200	519 points distributed regularly over space with increasing resolution toward the coast
English Channel	MOTHY (Daniel et al., 2011)	35	60-h simulations
Strait of Bonifacio	BOOM (Olita et al., 2012)	Huge number, not specified	1 spill/day from a tanker route corridor over 2008–2009
Coastal areas of Thailand	OILMAP (Singkran, 2013)	90	6-day simulations in 23 coastal provinces
New York and New Jersey	GNOME (Zelenke et al., 2012)	Defined by users	2-, 3-day simulations 2006–20xx
SANI area	MEDSLIK-II present work	Over 5000 spill/month	10-day simulations from the ship traffic maps over 2009–2013

It is used to predict the transport and diffusion of oil as well as oil transformation due to complex physical processes occurring at the sea surface.

The generalized active tracer equation for oil mixed in a marine environment is:

$$\frac{\partial C}{\partial t} = -\mathbf{U} \cdot \nabla C + \nabla C \cdot (\mathbf{K} \cdot \nabla C) + \sum_{j=1}^{M} r_j(C), \quad (1)$$

where $C(x, y, z, t)$ is the concentration of the oil as a function of space and time coordinates, normally with units of mass of substance over volume; $\frac{\partial}{\partial t}$ is the local time rate-of-change operator, $\mathbf{U}$ is the flow field with components (U, V, W); $\mathbf{K}$ is the diffusivity tensor which parameterizes turbulence effects, and $r_j(C)$ are the M transformation rates that modify the tracer concentration due to physical transformation processes at the seawater surface.

MEDSLIK-II calculates the advection–diffusion processes using a Lagrangian approach. The oil slick is discretized into constituent particles. Each particle moves due to currents, winds, and waves, and follows a trajectory calculated using:

$$\begin{aligned} dx(t) &= U(x, y, z, t)dt + dx'(t), \\ dy(t) &= V(x, y, z, t)dt + dy'(t), \\ dz(t) &= dz'(t), \end{aligned} \quad (2)$$

where $dx'(t),\ dy'(t)$ are the random walk displacements due to horizontal turbulent diffusion and $dz'(t)$ is due to vertical turbulent diffusion. Two components of the flow velocity, $\mathbf{U} = (U, V)$ are provided by the currents from the external model (MFS) with the addition of a Stokes drift-equivalent correction term that is taken to be simply proportional to the wind components multiplied by 0.01, in accordance with the work of Lehr et al. (2002) and Coppini et al. (2011).

The oil transformation processes at the surface are calculated by considering the entire oil slick volume subdivided into thick slick V^{TK} and thin slick V^{TN} parts (De Dominicis et al., 2013a). The changes in the surface oil volume are attributable to three main processes, known collectively as weathering. The first process is evaporation: the lighter fractions of oil disappear, while the remaining fractions can be dispersed below the water surface. Additionally, during the first 24 h, a given spill spreads mechanically over the water surface under the action of gravitational forces, the so-called spreading process. Finally, oil at the surface might be emulsified and dispersed below the surface, being lost forever due to sedimentation.

MEDSLIK-II uses the sea surface temperature provided by MFS to calculate the evaporation of oil from the sea surface. Evaporation leads to an increase in the viscosity of the oil, which influences dispersion of the oil in the water column.

If an oil particle arrives on the coast, the model is able to simulate the adsorption of particles into the coastal environment, taking into account a probability that oil may be washed back into the water (De Dominicis et al., 2013a).

As outputs, MEDSLIK-II provides the oil concentrations at the surface, in the dispersed fraction, and on the coast. Oil concentrations at the surface and in the dispersed fraction are calculated on a finer grid than the one used in the hydrodynamic model (De Dominicis et al., 2013a); in this work we used a resolution of 150 m. MEDSLIK-II calculates the oil concentration on the coast by using a coastline discretized into segments with a resolution appropriate for each segment, which varies from a few meters to a hundred meters for an almost straight coastal segment.

2.3. Meteo-oceanographic data

As detailed above, MEDSLIK-II requires the input of data about atmospheric winds, sea surface temperatures, and sea currents. The atmospheric wind data were provided by the European Centre for Medium-Range Weather Forecasts (ECMWF) analyses, at 0.25° horizontal and 6-h temporal resolution. The ocean current data were provided by daily analysis fields produced by the Mediterranean Forecasting System (MFS) at $1/16° \times 1/16°$ horizontal resolution and 71 unevenly spaced, vertical levels (Pinardi et al., 2003; Tonani et al., 2008; Oddo et al., 2009). The analyses are produced by a data assimilation system that uses satellite and *in situ* data (Dobricic and Pinardi, 2008).

3. Oil hazard mapping methodology

The oil hazard mapping methodology developed in this paper uses the following assumptions:

- the traffic density distribution and the amount of oil operationally spilled is representative of the present state and will not vary significantly in the future;
- the oil spill simulations, performed using the past daily meteo-oceanographic conditions from 2009 to 2013, sampled relevant possible meteo-oceanographic conditions.

Consequently, we think that evaluating the hazard maps using the data described in Section 2 can offer a tool to assess oil spill pollution event impacts in the future.

The oil hazard mapping methodology is composed of the following steps (Fig. 2):

(1) definition of the hypothetical oil spills (positions, starting dates, and number of oil spills) starting from the ship traffic maps; estimation of the oil quantity discharged along the selected shipping lanes (Section 3.1);
(2) oil spill model simulations (Section 3.2); and
(3) production of hazard maps (Section 3.3).

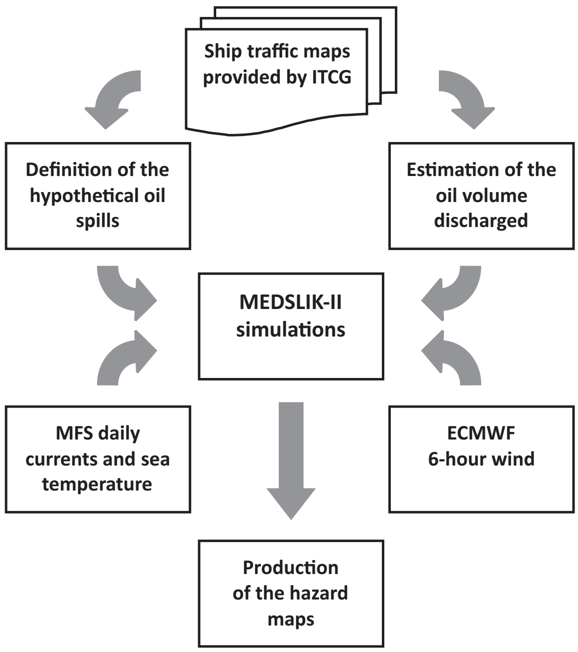

Fig. 2. A schematic diagram of the oil pollution hazard mapping methodology.

3.1. Definition of the oil spill scenarios

Starting with the ship traffic maps, the following input parameters have to be defined:

- the number of release points, N_p for the shipping lanes;
- the oil spill starting dates, S; and
- the hourly rate of oil spillage from each point, Q_r [ton/hour].

In order to estimate N_p, several experiments were performed by increasing the number of release points from 2000 to 7000 and studying the sensitivity of the simulations. The optimal N_p (5000) is reached when, adding 20% more release points does not produce significant changes in the simulation output.

In Table 2 the number of oil spills computed for each month are listed.

To sustain temporal continuity of the oil concentration fields a spin-up period of 10 days was introduced.

The dates S and starting positions X_p, Y_p can be extracted from the traffic density maps. Geographic coordinates of the virtual oil sources and starting dates of each spill are regarded as random variables. The dates are assumed to follow a uniform range distribution in time over the month. Spatial distributions of the hypothetical oil spills of a given month follow a given ship traffic density distribution; therefore, the majority of the random sources will be situated in the most frequently navigated routes. Segments of the main shipping routes are extracted from the traffic density maps and described by the geographical coordinates of the two end-points, the average traffic intensity, and the width of the ship route in relative units. Gaussian probability distributions are applied with respect to the width of the segments. Spatial–temporal randomization is used to produce the dates and positions of spills for each month.

The hourly rate of oil spillage, Q_r, from the N_p points can be evaluated using the information about the overall amount of oil discharged in a month in the SANI area. This can be calculated by combining the information about ship types with an estimation of the spilled oil in the entire Mediterranean Sea. Currently, an exact value is unavailable and an approximate value must be used. The estimated values obtained via aerial and satellite surveillance vary from 150,000 tons to 600,000 tons (REMPEC, 2002; Ferraro et al., 2007; Alexopoulos, 2008; Pisano, 2011). The annual oil discharge volume in the SANI area, Q_D, assuming that the oil related to operational pollution is discharged homogeneously over the Mediterranean Sea, is then calculated as:

$$Q_D = Q_T \frac{S_{SANI}}{S_{MED}}, \tag{3}$$

where Q_T is the annual total oil discharge volume in the Mediterranean, S_{SANI} is the surface area of the SANI, and S_{MED} is the surface of the Mediterranean area. Using 200,000 tons for the Mediterranean total discharge volume during 2009, (3) gives a discharged volume of 20,000 tons in the SANI area during 2009. The monthly ship traffic density distributions data provided by ITCG were used to obtain the monthly distribution of oil discharges. The traffic intensity index I_{TRF} can be introduced as follows:

$$I_{TRF} = \frac{I^M_{TRF}}{I^A_{TRF}}. \tag{4}$$

I^M_{TRF} is the monthly number of the ships in the SANI area according to the ship traffic density data, and I^A_{TRF} is the annual number of ships.

Multiplying the traffic intensity index by the annual oil discharge volume, the variability over time of the spilled oil volume caused by the temporal variability of ship traffic is obtained:

$$Q^M_D = I_{TRF} Q_D. \tag{5}$$

Fig. 3 (blue data) shows the monthly oil volumes discharged, which were obtained from (5), for the period 2010–2012.

Another alternative methodology to estimate the monthly distribution of oil discharges can be set up using ship type distributions data. In our case, we used the information on the number of different types of ships in the Ionian Sea and those that crossed the Otranto Strait during 4-month periods, provided by ITCG. The data covers 8 ship types (cargo ships, passenger ships, high speed craft, special craft, tankers, vessels, unknown, and other ships).

It is possible to define a ship index I_{SHIP}:

$$I_{SHIP} = \frac{I^M_{SHIP}}{I^A_{SHIP}}, \tag{6}$$

where I^M_{SHIP} is the monthly number of ships (all types, including tankers), and I^A_{SHIP} is the annual number of ships. From the monthly distribution of the ship index, it is possible to obtain another estimate of the monthly discharged oil (Ferraro et al., 2007):

$$Q^M_D = I_{SHIP} Q_D. \tag{7}$$

Table 2
Number of the individual oil spills computed by MEDSLIK-II on monthly basis in the SANI area.

Year/Month	January	February	March	April	May	June	July	August	September	October	November	December
2009		5192	5225	5235	5330	5232	5216	5100	5175	5131	5159	5197
2010	7370	5099	7320	7355	5279	7346	5222	5127	5225	5200	5199	5221
2011	5260	5147	5244	5239	5345	5234	5243	5356	5256	5263	7423	5111
2012	5254	5048	5066	5240	5343	5244	5241	5326	5250	5187	7413	5235
2013	5237	5140	5224	5253								

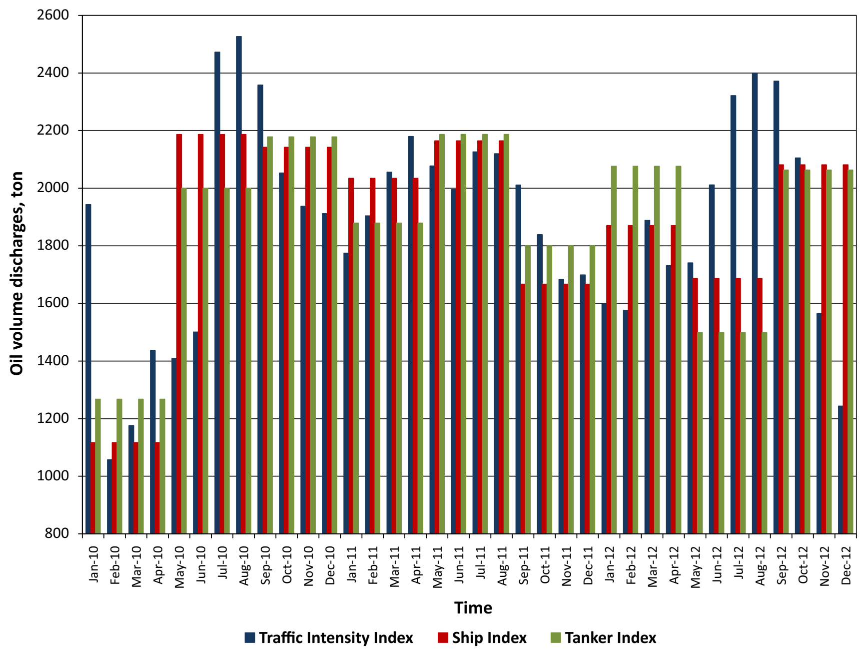

Fig. 3. Oil volumes discharged operationally in the SANI area obtained from the traffic intensity indexes (5) – blue data, from the ship indexes (7) – red data, and from the tanker indexes – green data. (For interpretation of the references to color in this figure legend, the reader is referred to the web version of this article.)

The monthly distribution of oil discharges calculated using (7) is shown in Fig. 3 (red data) and can be compared with the values given by (5).

Following the same approach, a tanker index can be estimated and, assuming that the majority of pollution is caused by tankers (Pavlakis et al., 2001), the monthly distribution of oil spill volume discharged from tankers can be estimated (Fig. 3, green data). Besides the approximation made in the calculations, quite a good agreement among the different data sets is obtained as is shown in Fig. 3. In the SANI area, temporal variability of traffic intensity index does not differ substantially from both ship and tanker indexes during 2009–2012.

In this work, we used Q_D^M obtained from (5) because the data on ship traffic density have higher spatial and temporal resolution than the data on ship and tanker indexes. However, (6) and (7) represent an alternative method that can be used if the ship traffic density distribution is not available.

The hourly rate of oil spillage, Q_r [ton/hour], from each of N_p points will be distributed throughout the year accordingly to the calculated monthly oil discharge distribution:

$$Q_r = \frac{Q_D^M}{N_P D}, \tag{8}$$

where D is the oil spill release duration. D has been set equal to 3 h; it is expected that this release time is long enough to form oil slicks that are the typical size and shape of those observed from satellites (Pavlakis et al., 2001).

3.2. Oil spill model simulations

After defining the oil spill scenarios it is necessary to define some additional simulation parameters:

- the length of the simulation, L, taken to be 240 h. This parameter corresponds to a possible realistic surface residence time of oil spilled at sea. The residence time of oil at sea is controlled by a combination of domain geometry, ocean currents, waves, turbulent diffusion, type of oil, and sea surface temperature (see details in De Dominicis et al. (2013a)). Based on the scale estimation and previous papers (Table 1) it is assumed that the period indicated above is long enough for the discharged oil to evaporate, disperse, or become beached;
- the type of oil was chosen based on the CEDRE technical newsletter (CEDRE, 2011). Crude oil with an API of 22 and a density of 919 kg m^{-3} is the type most frequently released.

Using MEDSLIK-II and the available oceanographic fields (daily analysis surface currents from MFS) and ECMWF meteorological fields, the transport, dispersion, and transformation of N_p oil spills in a month were analyzed. The simulation outputs were hourly distributions of oil concentration at the surface and at the coastline.

3.3. Hazard calculations

According to the UNESCO hazard definition (UNESCO, 1972) a dimensionless concentration function $THR_{HOUR}(x,y)$ can be defined as a function of hourly oil concentration $C_{HOUR}(x,y)$:

$$THR_{HOUR}(x,y) = \begin{cases} 1, & C_{HOUR}(x,y) > \overline{C} \\ 0, & C_{HOUR}(x,y) \leqslant \overline{C} \end{cases}, \tag{9}$$

where $\overline{C}$ is the threshold concentration, i.e., the value that, if exceeded, might lead to destructive events. The $\overline{C}$ values remain controversial because the concentration of oil that is destructive with regard to marine ecosystems has not yet been clarified (French McCay et al., 2004; Kirby and Law, 2010).

We will examine two dimensionless concentration functions, one for surface oil and another for beached oil. Two values of $\overline{C}$ are then considered: $\overline{C}^{SRF}$, the threshold concentration for the surface, chosen to be equal to 1 kg km^{-2}, and $\overline{C}^{CST}$, for the beached oil, set equal to 0.1 kg km^{-1}.

The hazard function $H(x,y)$ for surface or beached oil is then defined to be the likelihood frequency (expressed as a probability) written as:

$$H(x,y) = \frac{1}{M}\sum_{HOUR=1}^{M} THR_{HOUR}(x,y), \tag{10}$$

where M is the number of hours in a month. $H(x, y)$ clearly ranges between 0 and 1, where 1 indicates maximum hazard and 0 no hazard.

The hazard has been calculated on a grid of 30″, which is a good compromise between computational efficiency and accuracy of visualization.

It should be noted that in the hazard calculation methodology described above some important environmental processes have been neglected, including cumulative effects of small oil concentrations at coastline, accumulation in biota, and biogeochemical oil degradation. All of these issues need to be better understood and mathematically formalized, and should be taken into consideration in the next generation of hazard calculations.

4. Hazard mapping

Starting our analysis from the averaged 2009–2012 hazard maps for the sea surface and coastline (Fig. 4), we note that the surface spatial distribution of hazard tends to correspond to the locations of the main shipping routes. Average surface hazard distributions reveal distinctive "hot spots" in the Taranto Port area and in the semi-closed area between Corfu Island and the Greek coastlines (Fig. 4a). These areas might be chronically polluted by operational oil spills due to intense traffic in the areas and relatively weak circulation. Conversely, the Bari Port area does not reveal high surface hazard, because in that area the strong southeastern currents carry oil away from the shore. It is also interesting to notice that the shape of the largest average surface hazard area is following the climatological shape of the intense currents along the western Adriatic Sea, the so-called Western Adriatic Coastal Current (Artegiani et al., 1997; Oddo et al., 2005).

Table 3
Subdivision of the SANI area according to the magnitude of the mean oil surface hazard and standard deviation.

	Mean hazard	
	Low	High
Standard deviation		
Low	***I* – Permanently clean:** Northeast of Bari; Center of the Taranto Gulf; South of Corfu	***III* – Permanently polluted:** Offshore area in the southwestern Adriatic; along the axis of the Adriatic Coastal Current
High	***II* – Sporadically clean:** Between Bari and Brindisi; Southeastern Adriatic; Central part of the SANI area (near 39°N 19°E); Near Crotone	***IV* – Sporadically polluted:** Port of Taranto; Southwestern Adriatic; between Corfu and the Greek shoreline

As shown in Fig. 4c, we observe that the temporal variability of the maximum surface hazard area is moderate but that hazard variability is large in the near coastal areas and in the open ocean areas that show smaller average hazard values. According to the mean and standard deviation maps (Fig. 4a and c), the SANI area can be subdivided into four categories (I–IV): (I) is a sub-area of low mean and low standard deviation; (II) is a sub-area of low mean and high standard deviation; (III) is a sub-area of high mean and low standard deviation; and (IV) is a sub-area of high mean and high standard deviation (Table 3). Sub-area (I) includes the area northeast of Bari, the center of the Taranto Gulf, and the area south of Corfu. This sub-area seems to be permanently clean. Sub-

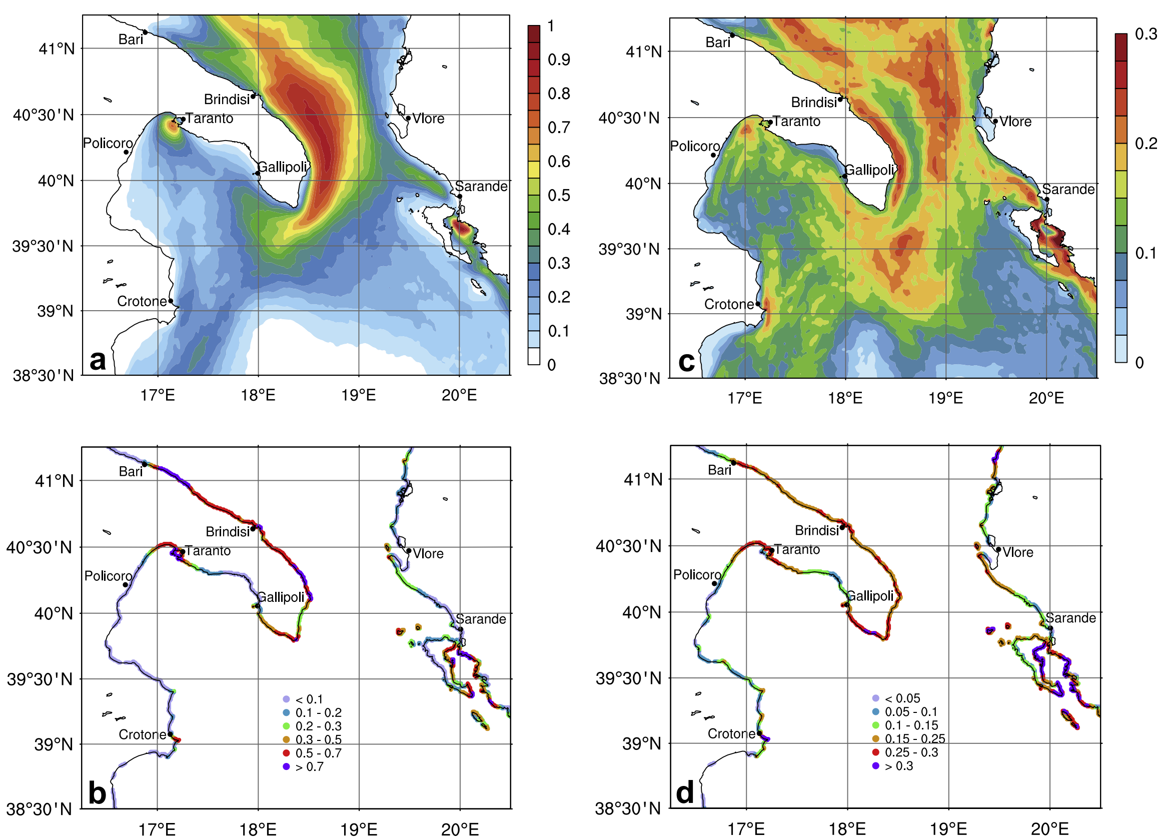

Fig. 4. (a) Averaged 2009–2012 hazard map at the sea surface and (c) its standard deviation. (b) Averaged 2009–2012 map of beached oil hazard at the coastline and (d) its standard deviation.

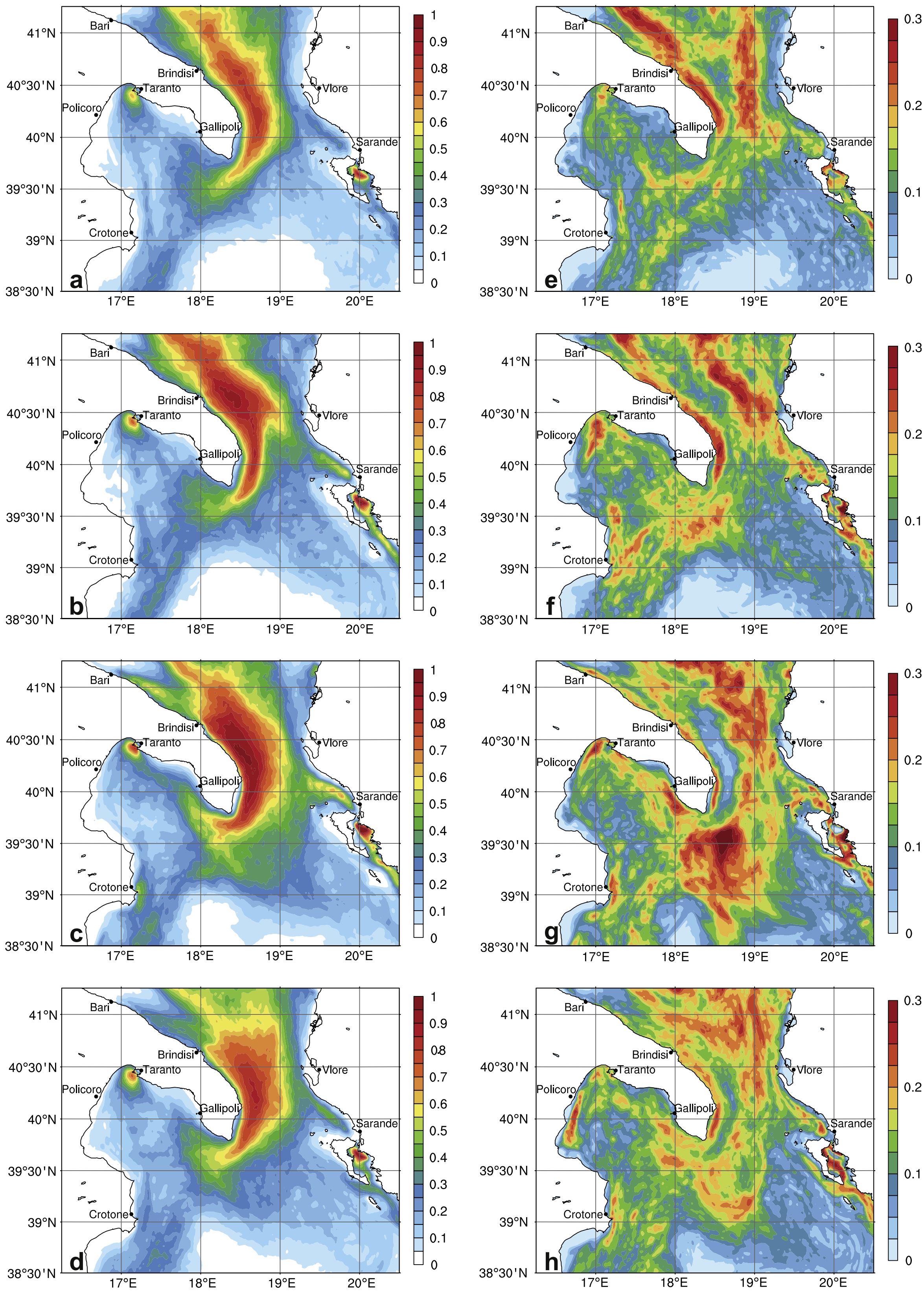

Fig. 5. Seasonally averaged surface hazard maps (left panel) and their standard deviations (right panel): (a), (e) winter; (b), (f) spring; (c), (g) summer; and (d), (h) autumn.

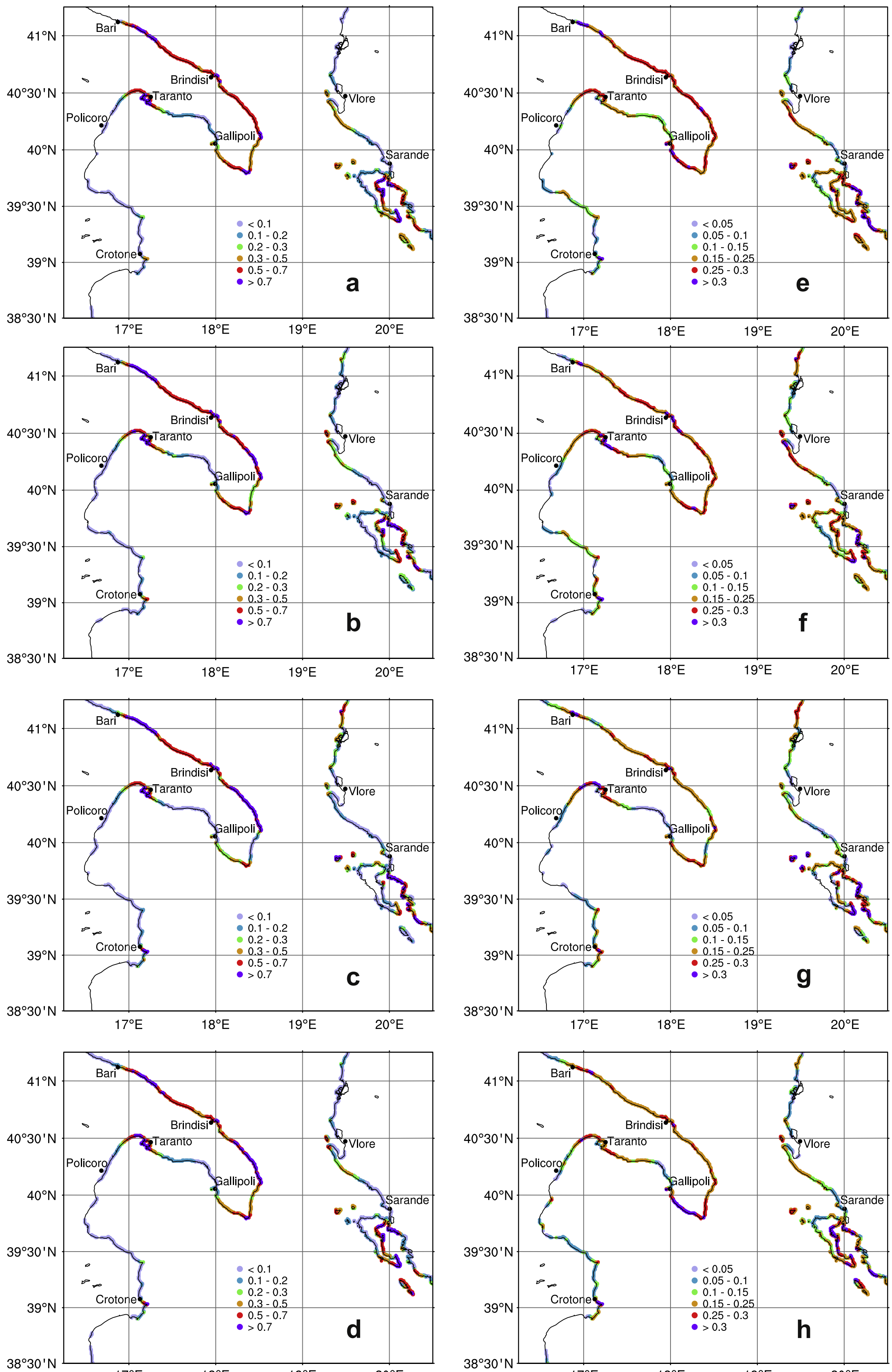

Fig. 6. Seasonally averaged coastline hazard maps (left panel) and their standard deviations (right panel): (a), (e) winter; (b), (f) spring; (c), (g) summer; and (d), (h) autumn.

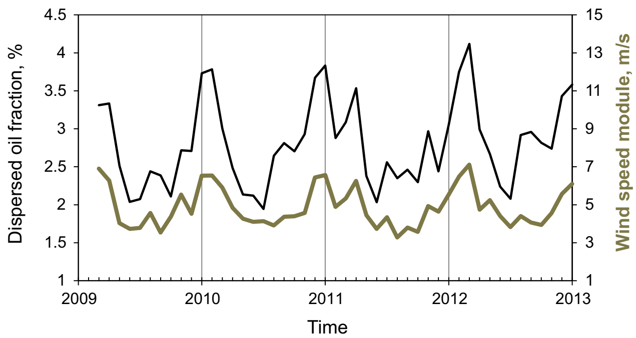

Fig. 7. Temporal variability of the average dispersed oil fraction and wind speed module over the SANI area.

area (II) includes the area between Bari and Brindisi, the southeast Adriatic; the central part of the SANI area (near 39°N 19°E), and the area near the Crotone Port. This sub-area seems to be sporadically clean. Sub-area (III) includes the southwest Adriatic that is continuously under severe pollution pressure. Sub-area (IV) includes the Taranto Port zone and the area between Corfu and the Greek shoreline.

Averaged over 2009–2012 coastline oil hazard maps (Fig. 4b and d) show moderate but persistent levels of pollution along the whole SANI coastline. The higher oil hazard areas of the coastline are found between Bari and Gallipoli. Shoreline segments southeast of Bari, in the vicinity of Brindisi, as well as the southwestern and southern tips of the Salento Peninsula demonstrate hazards that exceed 0.7. The same values are found in the Taranto Port, at the eastern coastline of Corfu Island, and along the opposing Greek coastline. In the case of coastline hazards, two types of coastlines can be distinguished: permanently polluted coastline, such as the Taranto Port and the coastline between Bari and Gallipoli, and sporadically polluted coastline, which encompasses the coastline near the Crotone Port, the Albanian coastline of the SANI, and the Corfu Island coastline. The southeastern shore on the Taranto Gulf demonstrates quite low levels of hazards with moderate variability (Fig. 4b and d). A very similar spatial distribution of Oil Spill Hazard Indexes concerning hydrocarbon maritime traffic was obtained by Garcia et al. (2013) for the Italian coastline of the SANI area.

The seasonally averaged 2009–2012 hazard distributions (Fig. 5) show approximately the same features as the annually averaged 2009–2012 surface hazard map (Fig. 4) and the temporal variability of the meteo-oceanographic conditions is also visible. The surface hazard seasonal maps indicate the lowest hazard in winter (Fig. 5a) and the highest in summer (Fig. 5c), which is probably due to more intense dispersion of the oil in the water column caused by higher wind intensity in winter than in summer. Indeed, as shown in Fig. 7, the dispersed oil fraction increases when the wind intensity is higher. As shown in Fig. 5c, during summer the high surface hazard area elongates into the Gulf of Taranto and areas of moderate hazards ($H \approx 0.5$) tend to spread southeastward to the center of the SANI area (at 39°N 19°E). Narrow local areas of enhanced hazard appear near the Albanian and Greek shores in summer.

The seasonal hazard maps for the coastline (Fig. 6) indicate high hazards at the whole coastline from Bari to Galipolli and in the Port of Taranto in every season. The eastern coastline of Corfu Island shows increased hazards in winter (Fig. 6a) and autumn (Fig. 6d). In the Port of Crotone, coastline hazards peak in summer (Fig. 6c) and also in autumn (Fig. 6d).

Monthly sea surface hazard maps reveal a significant spatial and temporal variability. December and June surface hazard distributions were selected to present the monthly variability (December 2009–2012 in Fig. 8 and June 2009–2012 in Fig. 9) together with the monthly mean current velocity fields. It is evident that part of the commonalities and differences between the monthly mean surface hazard map and the multi-year average patterns are connected with the horizontal structure of the general circulation. The majority of the oil spills from the high traffic shipping lanes in the southern Adriatic are under the direct influence of the Western Adriatic Coastal Current, resulting in the southeastward transport of pollution (Poulain, 2001; Zavatarelli et al., 2002; Zavatarelli and Pinardi, 2003), as shown in Figs. 8e, h and 9e, f. On the other hand, in the Ionian part of the SANI region the oil spills are controlled by a variable current system, dominated by mesoscale eddies of different intensities. Furthermore, one of the important differences between December and June is the weakening of oil dispersion in June, which is controlled by the seasonal wind cycle as shown in Fig. 7.

In December (Fig. 8), the western Adriatic high surface hazard area is broader than in June and it extends toward the center of the Otranto Strait (Fig. 1). The high hazard area near the Port of Taranto is shaped by the different intensities of the cyclonic circulation inside the Gulf of Taranto in the different years. A more intense cyclonic gyre in December 2009 (Fig. 8e) keeps the oil near the Port while different circulation patterns (a meandering jet in December 2012 (Fig. 8h), a weak meander in December 2010 (Fig. 8f), and unstructured weak currents in December 2011 (Fig. 8g)) enlarged the area of high surface hazard further offshore.

In June (Fig. 9), the high hazard area in the western Adriatic extends further inshore, toward the Bari and Brindisi coastlines, probably due to the lower intensity of the Western Adriatic Coastal Current system, which is very evident comparing the currents in Figs. 8g and 9g. In June, levels of hazard in the Gulf of Taranto are higher than in December due to the higher variability of the current field in summer with respect to the winter season and the fact that oil persists at the surface longer in June than in December due to the change in dispersion processes. Additionally, formation of high-hazard lenses in the Taranto Gulf is more common in June. Local and coastal differences in distribution of the high hazard areas arise from the increase in local shipping in this period and a generally weaker coastal circulation amplitude. Such features are found near the Crotone Port in June 2012 (Fig. 9d), and along the Albanian and Greek coastlines during June 2009–2012 (Fig. 9a–d).

Monthly hazard maps at the coastline (Fig. 10) reveal more spatial variability than the annual and seasonal maps, as in the case of the surface oil hazard. In the case of the coastlines, it is more difficult to find a connection between the hazard distributions and circulation patterns because the current data has a coarse resolution and shows peaks offshore. As shown in Fig. 10, hazards of more than 0.5 probability are always revealed in the Taranto Port and along the Greek coast opposite to Corfu. The eastern coast of Corfu Island and the Ionian coast of the Salento Peninsula are usually more polluted in December (Fig. 10a–d) than in June (Fig. 10e–h), while the Adriatic coast of the Salento Peninsula presents a higher hazard during June. Local differences include episodic hazards at the coastline of Taranto Gulf: near Galipolli (quite frequent, in December 2009, 2010, 2012 as shown in Fig. 10d; and in June 2009 and 2011 as shown in Fig. 10e and g), Policoro (rather rare, in June 2009, 2010, and 2012, as shown in Fig. 10e, f, and h), and Crotone (very rare, in December 2011, and June of both 2009 and 2012, as shown in Fig. 10).

As Fig. 10 indicates, some important Marine Protected Areas (MPA) could be affected by operational oil pollution including (3) Torre Guaceto MPA (Italy), (5) Butrinti National Park (Albania), and (6) Kalama Delta Natural Reserve (Greece). The sites of (1) Capo Rizzuto MPA (Italy), (2) Porto Cesareo MPA (Italy), and (4) Vjose-Narte Landscape Protection Site (Albania) are affected in

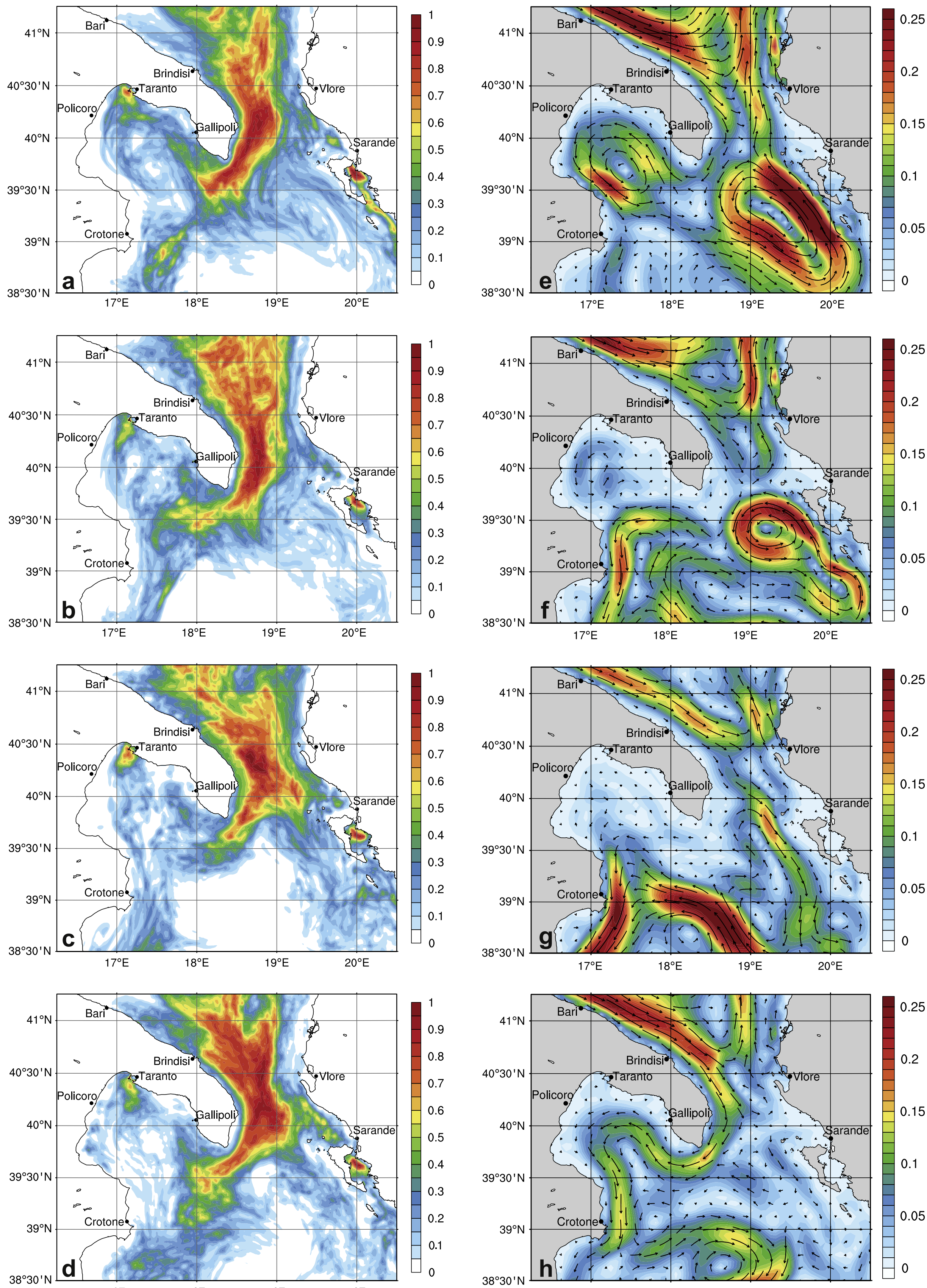

Fig. 8. Monthly averaged surface hazard maps (left panel) and surface currents (right panel) during December of: 2009 (a), (e); 2010 (b), (f); 2011 (c), (g); and 2012 (d), (h).

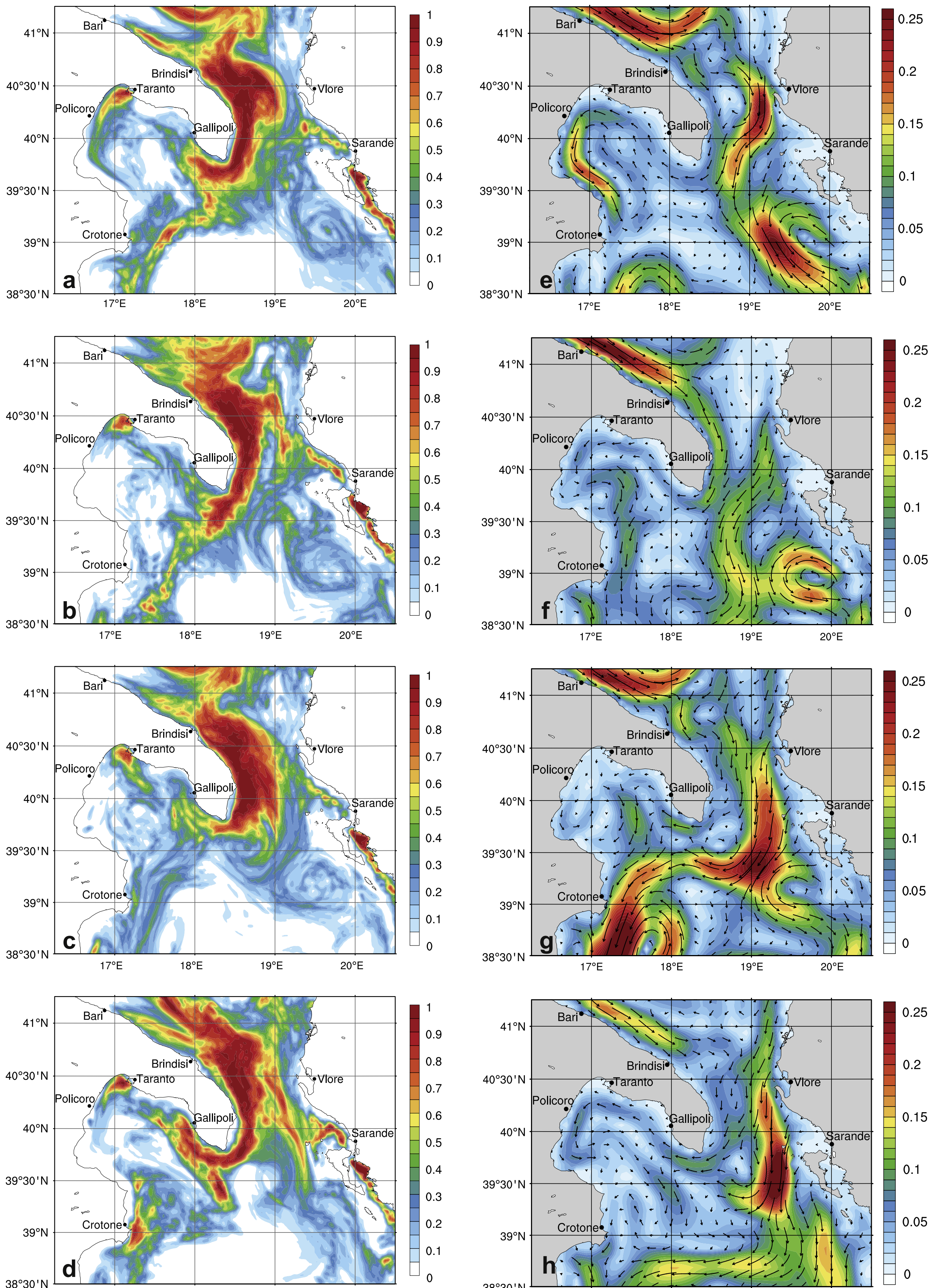

Fig. 9. Monthly averaged surface hazard maps (left panel) and surface currents (right panel) during June of: 2009 (a), (e); 2010 (b), (f); 2011 (c), (g); and 2012 (d), (h).

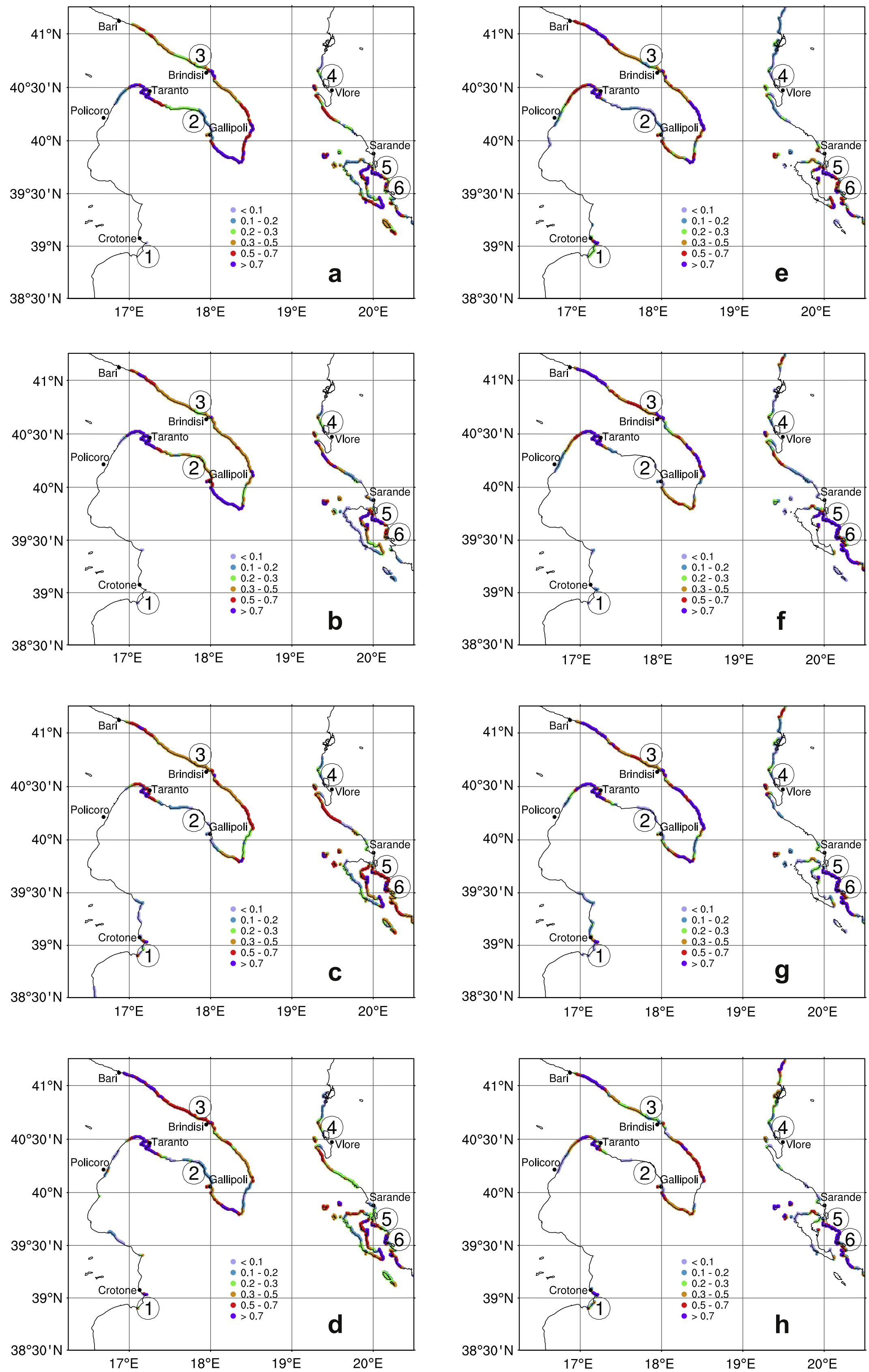

Fig. 10. Monthly averaged hazard maps at the coastline during December (left panel): 2009 (a); 2010 (b); 2011 (c); 2012 (d); and during June (right panel): 2009 (e); 2010 (f); 2011 (g); and 2012 (h). Marine protected areas are indicated by the circled numbers 1–6.

December and June episodically. These sites are defined in the GIS Mediterranean Marine Protected Areas database (MAPAMED, 2012).

5. Conclusion

A new methodology was developed to obtain oil pollution hazard maps for operational oil spill events. The simulated concentrations were combined to produce sea surface and coastline hazard maps at different levels of time resolution (time mean, seasonal, and monthly).

The methodology is based on combining ship traffic density maps provided by ITCG with the MFS ocean circulation model, ECMWF winds and the MEDSLIK-II oil spill model. The methodology is applied to the SANI region, and relies on statistically confident simulations. Overall, several hundred thousand MEDSLIK-II simulations were performed for the 2009–2013 time period.

The hazard maps obtained can be considered representative of future events because we can assume that the traffic density distribution and the amount of oil operationally spilled is representative of the present state and will follow the estimated tendencies (Fig. 3) in the future, and the historical database of meteo-oceanographic conditions contains a realistic sample of possible weather and sea state conditions.

On long-term time-mean scales, the spatial distribution of hazard at the sea surface tends to correspond to the oil source distribution (i.e., the main shipping route locations). Furthermore, the shape of the largest average surface hazard area follows the climatological shape of the Western Adriatic Coastal Current. The areas of highest hazard are located in the southwest Adriatic Sea and in distinctive "hot spots" in the Taranto Port area and in the semi-closed area between Corfu Island and the Greek coastline. Averaged over 2009–2012 coastline hazard maps show moderate but persistent levels of pollution hazard along the whole coastline of the Salento Peninsula as well as the Greek coastline opposite Corfu Island. The coastal segments of the highest hazard ($H > 0.7$) are found southeast of Bari, in the vicinity of Brindisi; at the southwestern and southern tips of the Salento Peninsula; and in the Taranto Port and the Greek coastline opposite Corfu Island.

On seasonal time-mean scales, the surface hazard is lower during winter and higher during summer, due to the higher wind intensity in winter that causes a more intense dispersion of the oil in the water column. The results indicated dispersion makes a substantial contribution to the surface hazard seasonality, which is a result of the temporal wind speed variability. That is why to obtain the hazard variability on these scales a full oil spill model should be used rather than applying any simplifications to the oil weathering simulations.

Monthly hazard maps at the sea surface demonstrate the most significant spatial and temporal variability, indicating a direct connection with the monthly varying meteo-oceanographic conditions. It has been shown that the hazard distributions in the southern Adriatic are under the direct influence of the varying Western Adriatic Coastal Current (Poulain, 2001; Zavatarelli et al., 2002; Zavatarelli and Pinardi, 2003). In the Ionian Sea, surface hazard is controlled by the high mesoscale variability of the flow field. The distribution of hazards in the interior Taranto Gulf is mainly influenced by the variability of the cyclonic circulation.

Although in the case of the coastlines it is more difficult to find a connection between the hazard distributions and the circulation patterns, monthly oil hazard calculations reveal that a number of the marine protected areas could be chronically affected by operational oil spill pollution.

The oil pollution hazard maps obtained allow comparison with the results of aerial and satellite oil spill monitoring and coastline sampling and are found to be in good qualitative agreement with the previous data (Pavlakis et al., 2001; Ferraro et al., 2007). The methodology developed is applicable to any area and allows further development related to advances in the model representation of natural processes and improvements in oil spill modelling.

The oil hazard calculation methodology needs further improvement including the formalization of many important environmental processes, namely the cumulative effect of low oil concentrations at the coastline, accumulation in biota, and biogeochemical oil degradation. Furthermore, we believe that in the future higher resolution current data will improve the representation of the coastline hazards.

Acknowledgements

We thank ITCG for providing the ship traffic data. This work was performed in the framework of the IONIO Research Project (IONian Integrated marine Observatory) co-funded by the European Territorial Cooperation Programs JTS Greece–Italy 2007–2013 (Contract No. I1.22.05). M. De Dominicis and N. Pinardi were supported by the MEDESS-4MS Project (Mediterranean Decision Support System for Marine Safety, Ref. 2S-MED11-01) co-financed by the European Regional Development Fund through the MED Programme and P. Oddo was supported by the RITMARE Project (La ricerca Italiana per il mare) funded by the Italian Ministry of University and Research.

References

Abascal, A., Castanedo, S., Medina, R., Liste, M., 2010. Analysis of the reliability of a statistical oil spill response model. Mar. Pollut. Bull. 60, 425–442.
Alexopoulos, A., 2008. Managing and assessing oil spills through systematic methods. Middle East Forum, 111–121.
Artegiani, A., Bregant, D., Paschini, E., Pinardi, N., Raicich, F., Russo, A., 1997. The Adriatic Sea general circulation. Part II: Baroclinic circulation structure. J. Phys. Oceanogr. 27, 1515–1532.
Barker, C., Galt, J., 2000. Analysis of methods used in spill response planning: Trajectory Analysis Planner TAP II. Spill Sci. Technol. Bull. 6, 145–152.
CEDRE, 2011. Review of spills having occurred worldwide in 2011. Sea Shore Tech. Newslett., 1–20.
Coppini, G., De Dominicis, M., Zodiatis, G., Lardner, R., Pinardi, N., Santoleri, R., Colella, S., Bignami, F., Hayes, D., Soloviev, D., Georgiou, G., Kallos, G., 2011. Hindcast of oil spill pollution during the Lebanon Crisis, July–August 2006. Mar. Pollut. Bull. 62, 140–153.
Daniel, P., Paradis, D., Ulvoas, V., 2011. Probabilistic products to support oil spill forecasts. In: EMS Annual Meeting, p. 100.
De Dominicis, M., Pinardi, N., Zodiatis, G., Lardner, R., 2013a. MEDSLIK-II, a Lagrangian marine surface oil spill model for short term forecasting – Part 1: theory. Geosci. Model Dev. 6, 1851–1869.
De Dominicis, M., Pinardi, N., Zodiatis, G., Archetti, R., 2013b. MEDSLIK-II, a Lagrangian marine surface oil spill model for short-term forecasting – Part 2: numerical simulations and validations. Geosci. Model Dev. 6, 1871–1888.
Dobricic, S., Pinardi, N., 2008. An oceanographic three-dimensional variational data assimilation scheme. Ocean Model. 22, 89–105.
Ferraro, G., Bernardini, A., David, M., Meyer-Roux, S., Muellenhof, O., Perkovic, M., Tarchi, D., Tpouzelis, K., 2007. Towards an operational use of space imagery for oil pollution monitoring in the Mediterranean basin: a demonstration in the Adriatic Sea. Mar. Pollut. Bull. 54, 403–422.
French, D., Schuttenberg, H., Tatsusaburo, I., 1999. Probabilities of oil exceeding thresholds of concern: examples from an evaluation for Florida Power and Light. In: AMOP 99 Technical Seminar, pp. 655–681.
French McCay, D., Rowe, J., Whittier, N., Sankaranarayanan, S., Etkin, D.S., 2004. Estimation of potential impacts and natural resource damages of oil. J. Hazard. Mater. 107, 11–25.
Galt, J., Payton, D., 1999. Development of quantitative methods for spill response planning: a trajectory analysis planner. Spill Sci. Technol. Bull. 5, 17–28.
Garcia, D.A., Bruschi, D., Cumo, F., Gugliermetti, F., 2013. The Oil Spill Hazard Index (OSHI) elaboration. An oil spill hazard assessment concerning Italian hydrocarbons maritime traffic. Ocean Coast. Manage. 80, 1–11.
Grifoll, M., Jord, G., Borja, A., Espino, M., 2010. A new risk assessment method for water quality degradation in harbour domains, using hydrodynamic models. Mar. Pollut. Bull. 60, 69–78.
Kirby, M., Law, R., 2010. Accidental spills at sea – risk, impact, mitigation and the need for co-ordinated post-incident monitoring. Mar. Pollut. Bull. 60, 797–803.

Lehr, W., Jones, R., Evans, M., Simecek-Beatty, D., 2002. Revisions of the ADIOS oil spill model. Model. Softw. 17, 191–199.
MAPAMED, 2012. The Database on Mediterranean Marine Protected Areas. MedPAN, RAC/SPA.
Oddo, P., Pinardi, N., Zavatarelli, M., 2005. A numerical study of the interannual variability of the Adriatic Sea (2000–2002). Sci. Total Environ. 353, 39–56.
Oddo, P., Adani, M., Pinardi, N., Fratianni, C., Tonani, M., Pettenuzzo, D., 2009. A nested Atlantic–Mediterranean Sea general circulation model for operational forecasting. Ocean Sci. Discuss. 6, 1093–1127.
Olita, A., Cucco, A., Simeone, S., Ribotti, A., Fazioli, L., Sorgente, B., Sorgente, R., 2012. Oil spill hazard and risk assessment for the shorelines of a Mediterranean coastal archipelago. Ocean Coast. Manage. 57, 44–52.
Pavlakis, P., Tarchi, D., Sieber, A., Ferraro, G., Vincent, S., 2001. On the Monitoring of Illicit Discharges – A Reconnaissance Study in the Mediterranean Sea. European Commission, EUR 19906 EN.
Pinardi, N., Allen, I., Demirov, E., De Mey, P., Korres, G., Lascaratos, A., Le Traon, P., Maillard, C., Manzella, G., Tziavos, C., 2003. The Mediterranean ocean forecasting system: first phase of implementation (1998–2001). Ann. Geophys. 21, 3–20.
Pisano, A., 2011. Development of Oil Spill Detection Techniques for Satellite Optical Sensors and Their Application to Monitor Oil Spill Discharge in the Mediterranean Sea. Ph.D. Thesis, University of Bologna.
Pizzigalli, C., Rupolo, V., Lombardi, E., Fratianni, C., Blanke, B., 2007. Seasonal variability dispersion maps in the Mediterranean Sea obtained from the Mediterranean Forecasting System Eulerian velocity fields. Prog. Oceanogr. 22, C05012, 1–17.
Poulain, P.M., 2001. Adriatic sea surface circulation as derived from drifter data between 1990 and 1999. J. Mar. Syst. 29, 3–32.
Price, J., Jonson, W., Marshall, C., Ji, Z., Rainey, G., 2003. Overview of the Oil Spill Risk Analysis (OSRA) model for environmental impact assessment. Spill Sci. Technol. Bull. 8, 529–533.
Price, J., Jonson, W., Marshall, C., Ji, Z., Rainey, G., 2004. Sensitivity testing for improved efficiency of a statistical oil-spill risk analysis model. Environ. Model. Softw. 19, 671–679.
REMPEC, 2002. Protecting the Mediterranean Against Maritime Accidents and Illegal Discharges from Ships. REMPEC.
REMPEC, 2008. Study of Maritime Traffic Flows in the Mediterranean Sea. REMPEC.
Ronza, A., Carol, S., Espejo, V., Vlchez, J., Arnaldos, J., 2006. A quantitative risk analysis approach to port hydrocarbon logistics. J. Hazard. Mater. 128, 10–24.
Samuels, W., Amstutz, D., Bahadur, R., Ziemniak, C., 2013. Development of a global oil spill modeling system. Earth Sci. Res. J. 2, 52–61.
Singkran, N., 2013. Classifying risk zones by the impacts of oil spills in the coastal waters of Thailand. Mar. Pollut. Bull. 70, 34–43.
Tarchi, G., Bernardini, A., Ferraro, G., Meyer-Roux, S., Muellenhoff, O., Topouzelis, K., 2006. Satellite Monitoring of Illicit Discharges from Vessels in the Seas around Italy 1999–2004. European Commission, EUR 22190 EN.
Tonani, M., Pinardi, N., Dobricic, S., Pujol, I., Fratianni, C., 2008. A high-resolution free-surface model of the Mediterranean Sea. Ocean Sci. 4, 1–14.
UNESCO, 1972. Report of Consultative Meeting of Experts on Statistical Study of Natural Hazards and Their Consequences. UNESCO.
Zavatarelli, M., Pinardi, N., 2003. The Adriatic Sea modelling system: a nested approach. Ann. Geophys. 21, 345–364.
Zavatarelli, M., Pinardi, N., Kourafalou, V.H., Maggiore, A., 2002. Diagnostic and prognostic model studies of the Adriatic Sea general circulation: seasonal variability. J. Geophys. Res. 107, C13004, 1–20.
Zelenke, B., O'Connor, C., Barker, C., Beegle-Krause, C.J., Eclipse, L., 2012. General NOAA Operational Modeling Environment (GNOME) Technical Documentation. U.S. Dept. of Commerce, NOAA Technical Memorandum NOS OR and R 40. Seattle, WA: Emergency Response Division, NOAA.